

‘Zwicky’s Nonet’: a compact merging ensemble of nine galaxies and 4C 35.06, a peculiar radio galaxy with dancing radio jets

K.G. Biju^{1,5*}, Joydeep Bagchi^{2†}, Ishwara-Chandra C.H.³, M. Pandey-Pommier⁴, Joe Jacob⁵, M.K. Patil⁶, Sunil Kumar P.⁷, Mahadev Pandge^{8‡}, Pratik Dabhade^{2§}, Madhuri Gaikwad³, Samir Dhurde², Sheelu Abraham², M. Vivek⁹, Ashish A. Mahabal¹⁰, S. G. Djorgovski¹⁰

¹ WMO Arts & Science college, Muttill, Wayanad, Kerala, 673122, India

² Inter University Centre for Astronomy and Astrophysics, (IUCAA), Pune University Campus, Post Bag 4, Pune 411007, India

³ National Centre for Radio Astrophysics, TIFR, Post Bag No. 3, Ganeshkhind, Pune, 411007, India

⁴ Centre de Recherche Astrophysique de Lyon- Observatoire de Lyon, 9 avenue Charles André, Saint-Genis Laval, F-69230, France

⁵ Newman College, Thodupuzha, Kerala, 685584, India

⁶ School of Physical Sciences, Swami Ramanand Teerth Marathwada University, Nanded, 431606, India

⁷ P.T.M.Govt. College, Perinthalmanna, Kerala, India

⁸ Department of Physics, Dayanand Science College, Latur, 413512, India

⁹ Department of Physics and Astronomy, University of Utah, Salt Lake City, UT 84112, USA

¹⁰ California Institute of Technology, 1200 E California Bl., Pasadena, CA 91125, USA

Accepted 2017 June 11. ; Received 2017 June 11; in original form 2016 July 12

ABSTRACT

We report the results of our radio, optical and infra-red studies of a peculiar radio source 4C 35.06, an extended radio-loud AGN at the center of galaxy cluster Abell 407 ($z = 0.047$). The central region of this cluster hosts a remarkably tight ensemble of nine galaxies, the spectra of which resemble those of passive red ellipticals, embedded within a diffuse stellar halo of ~ 1 arcmin size. This system (named the ‘Zwicky’s Nonet’) provides unique and compelling evidence for a multiple-nucleus cD galaxy precursor. Multifrequency radio observations of 4C 35.06 with the Giant Meterwave Radio Telescope (GMRT) at 610, 235 and 150 MHz reveal a system of 400 kpc scale helically twisted and kinked radio jets and outer diffuse lobes. The outer extremities of jets contain extremely steep spectrum (spectral index -1.7 to -2.5) relic/fossil radio plasma with a spectral age of a few $\times (10^7 - 10^8)$ yr. Such ultra-steep spectrum relic radio lobes without definitive hot-spots are rare, and they provide an opportunity to understand the life-cycle of relativistic jets and physics of black hole mergers in dense environments. We interpret our observations of this radio source in the context of the growth of its central black hole, triggering of its AGN activity and jet precession, all possibly caused by galaxy mergers in this dense galactic system. A slow conical precession of the jet axis due to gravitational perturbation between interacting black holes is invoked to explain the unusual jet morphology.

Key words: Galaxies: clusters: individual (Abell 407) , galaxies: elliptical and lenticular, cD, galaxies: jets-quasars: supermassive black holes- Radio continuum: galaxies.

1 INTRODUCTION

Galaxy mergers, which take place more frequently in the dense environments of galaxy clusters play a pivotal role in the evolution of galaxies in the Universe across cosmic time. The merger dynamics is influenced by various factors such as size, mass, impact parameter, relative velocity, gas con-

* kgbiju42@gmail.com

† joydeep@iucaa.in

‡ DST INSPIRE Faculty

§ Research Fellow, Indo-French Centre for the Promotion of Advanced Research (IFCPAR)/(CEFIPRA)

tent and the relative inclination of the participating galaxies. Mergers have profound effects on the properties of galaxies on various physical scales. On galactic scales ($\sim 10 - 100$ kpc) mergers may result in ram pressure stripping of gas, the formation of long tidal tails and enhanced star formation. On smaller scales (< 1 pc), the growth of black holes (BHs) and possible triggering of AGN activity with occasional relativistic jet ejection may occur in mergers, which transport matter and energy from the galaxy interiors to the surroundings through AGN feedback processes (McNamara & Nulsen 2012). On the smallest scales ($<< \text{pc}$), the final inspiral stage of merging BHs results in powerful gravitational wave emission. However, the formation and merger rates of galactic BHs are still much uncertain. Finally, on very large scales ($\sim 100 - 1000$ kpc), the shocks and turbulence inducted into the intra-cluster medium (ICM) during mergers may inject large amounts of nonthermal energy and subsequent shock heating of the ICM to X-ray temperatures, with disruption of cooling cores (Subramanian et al. 2006; McNamara & Nulsen 2007; Paul et al. 2011). Therefore cluster centers are fascinating laboratories to study galaxy formation and evolution.

Rich galaxy clusters are usually dominated by massive, luminous central elliptical galaxies known as the Brightest Cluster Galaxies (BCG). There are some interesting examples, where extremely massive ($> 10^{12} M_{\odot}$) and brighter ellipticals called the cD galaxies form in the densest regions near the spatial and kinematical center of their host clusters (Tovmassian & Andernach 2012; Garijo et al. 1997). The distinguishing property of cD galaxies is the presence of a diffuse, faint stellar halo that may extend up to 100s of kpc, well into the intracluster medium (Garijo et al. 1997; Tovmassian & Andernach 2012). These facts seem to suggest that the formation of cD galaxies is unique to the cluster environment and is linked closely to its dynamical history. It is still far from clear how cD galaxies originate in such a galactic environment, because very few clusters with cD galaxies in the process of formation have been identified.

cD galaxies are almost always radio loud and often eject powerful radio jets from accreting supermassive black holes (Bagchi & Kapahi 1994; McNamara & Nulsen 2007). Galaxy interactions and major mergers remove significant amounts of angular momentum by gravitational torque and drive a part of the constituent gas towards nuclear supermassive black holes (SMBHs), thereby triggering the activity of the central engine (Wilson & Colbert 1995). As a result, cD galaxies are more likely to be radio-loud above radio luminosity $\sim 10^{24.5} \text{ W Hz}^{-1}$ at 1.4 GHz compared with other galaxies in a cluster (Bagchi & Kapahi 1994). The multiple galactic nuclei observed in cDs and BCGs provide evidence supporting the merger scenario. In addition, the SMBHs of these galaxies are believed to grow by multiple galactic mergers (Volonteri et al. 2003; Kulkarni & Loeb 2012; Deane et al. 2014). Thus, gravitational perturbations in the accretion disc in the presence of closely spaced massive black hole pairs may result in the occurrence of distorted radio jets. The inversion symmetry found in ‘S’ or ‘Z’-shaped radio sources is ascribed to the precession of a spinning black hole (Deane et al. 2014; Begelman et al. 1980) and the associated tilting/perturbation in the accretion disk (Lu 1990;

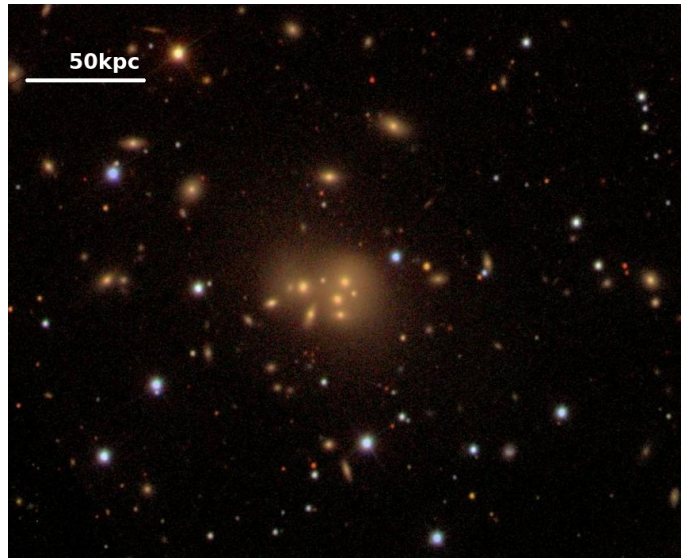


Figure 1. Colour image ($5.6' \times 4.7'$) of the galaxy cluster Abell 407 taken from the Sloan Digital Sky Survey (SDSS). The central region is host to a striking group of nine close packed galaxy like condensations, embedded within a diffuse stellar halo of intra-cluster light (the ‘Zwicky’s Nonet’). This system possibly represents an exceptionally rare site of a multiple-nucleus cD galaxy precursor assembling in a rich galaxy cluster environment.

Janiuk et al. 2008). The precessing radio jets in this situation are likely to trace a characteristic helical pattern on the sky (Gower et al. 1982). One prominent object showing this rare phenomenon is PKS 2149-158, a dual radio-loud elliptical galaxy pair in the center of cluster Abell 2382, forming a pair of twisted jet systems (Guidetti et al. 2008). The well known ‘C’-shaped wide-angle tail (WAT) source 3C 75 is another striking example of twin AGN producing two pairs of jets showing oscillations and interactions (Owen et al. 1985).

In this article, we report radio, optical and near-IR studies of the extraordinary radio source 4C 35.06 (B2 0258+35B), located near the center of the cluster Abell 407, which, interestingly, also harbors a remarkably compact group of nine galaxies embedded inside a diffuse stellar halo of faint intra-cluster light. We make a detailed study of this remarkable system, which possibly provides a unique and compelling evidence for an ongoing formation of a giant cD galaxy at the cluster center and connects to the evolution of its central black hole by mergers. The radio source 4C 35.06 clearly shows a very peculiar twisted jet system on 100 kpc scale, which we investigate further with multi-frequency radio data.

This paper is organised as follows; In Section 2 we discuss the optical, near-IR, radio and X-ray properties of the system. In Section 3 we discuss the observations and the data reduction procedure. In Section 4 the main results obtained in the present study are discussed in seven subsections. In the last concluding section, section 5, we summarise our findings. Throughout this article, a Hubble constant $H_0 = 73 \text{ kms}^{-1} \text{ Mpc}^{-1}$, and cosmological parameters $\Omega_M = 0.27$ and $\Omega_{\Lambda} = 0.73$ were used. For redshift $z = 0.047$ it implies the linear scale of $0.885 \text{ kpc arcsec}^{-1}$ and a luminosity distance of 200 Mpc (Wright 2006). We define the synchrotron emis-

Table 1. Galaxy properties in central region of Abell 407 cluster.

Galaxy ^a	Coordinates (J2000) (from SDSS)	Redshift ^b	SDSS Magnitudes					SDSS Colours		
			<i>u</i>	<i>g</i>	<i>r</i>	<i>i</i>	<i>z</i>	<i>g - r</i>	<i>r - i</i>	<i>i - z</i>
G1 (B)	03h 01m 51.5s +35d 50m 30s	0.0483	18.23	15.84	14.72	14.23	13.84	1.12	0.49	0.39
G2 (A)	03h 01m 51.2s +35d 50m 22s	0.0454	21.09	19.04	18.46	17.95	17.54	0.58	0.51	0.41
G3 (D)	03h 01m 51.8s +35d 50m 20s	0.0471	18.11	16.00	15.00	14.44	13.97	1.00	0.56	0.47
G4 (C)	03h 01m 51.7s +35d 50m 12s	0.0501	20.91	18.81	17.76	17.37	16.90	1.05	0.39	0.47
G5 (F)	03h 01m 51.5s +35d 50m 12s	0.0478	20.02	17.93	16.86	16.31	15.85	1.07	0.55	0.46
G6 (E)	03h 01m 52.4s +35d 50m 29s	0.0444	21.33	19.93	19.11	18.70	18.18	0.82	0.41	0.52
G7 (G)	03h 01m 53.2s +35d 50m 26s	0.0471	18.37	16.34	15.31	14.80	14.39	1.03	0.51	0.41
G8 (H)	03h 01m 53.7s +35d 50m 28s	-	-	-	-	-	-	-	-	-
G9 (I)	03h 01m 54.5s +35d 50m 18s	0.0451	20.27	18.68	17.59	17.23	16.68	1.09	0.36	0.55

^a Zwicky’s original nomenclature is shown within brackets.

^b From Schneider & Gunn (1982).

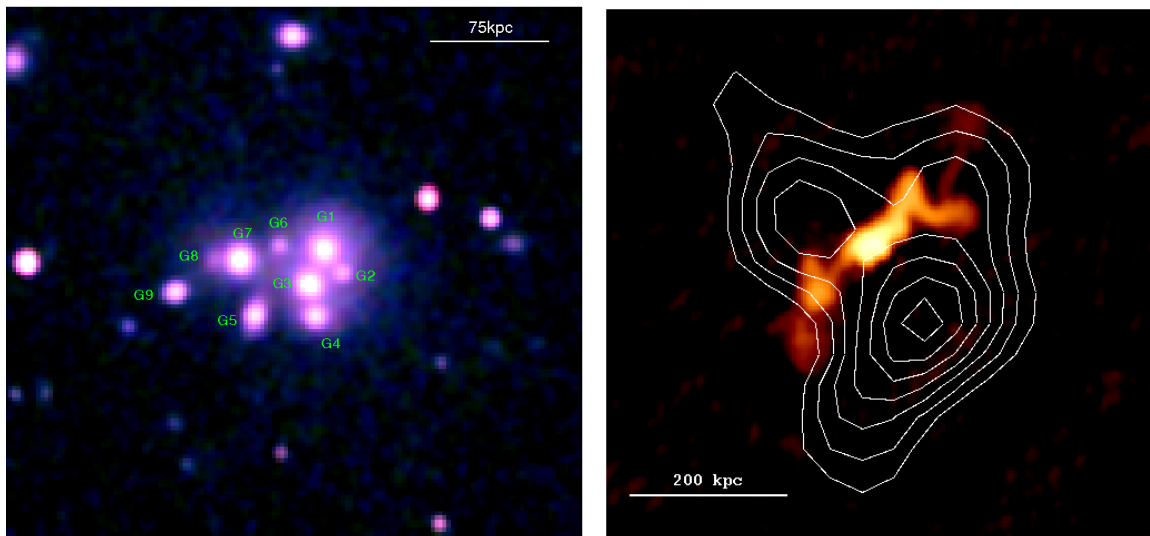


Figure 2. Left panel: A pseudo-color near infra-red image ($2.1' \times 2.1'$) of the compact group ‘Zwicky’s Nonet’ obtained by combining the J, H and K-band images available in the 2MASS 6X deep survey. The nine central galaxies of the nonet are marked on the image while Table 1 and Table 3 show their positions, magnitudes, colours and estimated central black hole masses. Right Panel: GMRT 150 MHz radio image ($11' \times 11'$) of 4C 35.06 is shown superposed on the ROSAT 0.5 - 2.4 keV band smoothed X-ray data shown with contours.

sion spectral index α by $S(\nu) \propto \nu^\alpha$, where $S(\nu)$ is the flux density at frequency ν .

2 ‘ZWICKY’S NONET’: PREVIOUS OPTICAL, X-RAY AND RADIO OBSERVATIONS

Abell 407 is a rich galaxy cluster of Bautz-Morgan class II, at a redshift of 0.047 (Abell et al. 1989). The optical image of the central region of this cluster from Sloan Digital Sky Survey (SDSS) shows a complex ensemble of at least nine galaxy-like condensations $\sim 1'$ across (~ 50 kpc), embedded in a low surface brightness, diffuse stellar halo, which is reminiscent of a giant cD galaxy (Figure 1). Table 1 lists the SDSS optical magnitudes, redshifts and colours of these nine galaxies. The $g - r$ colour index of ~ 1 indicates they are passive, early-type red galaxies. Historically, Fritz Zwicky first noticed this extraordinary galactic configuration (V Zw 311) in 1971 (Zwicky & Zwicky 1971); which was later studied in more detail by Schneider & Gunn (1982)

using the Palomar 200-inch and 60-inch telescopes. Schneider & Gunn (1982) described it as the “most nightmarish known multiple-nucleus system” and concluded that this puzzling galactic system possibly represents an extremely rare and unique snapshot of a giant cD galaxy caught in its formative stages. There were no further investigations of this highly unusual galactic system to understand its nature. Here we propose to name this extraordinary galaxy group of nine galaxies as ‘Zwicky’s Nonet’, honoring Fritz Zwicky who first noticed this galaxy group. To our knowledge, this is the most compact and rich system of multiple galaxies known to date. Some other famous compact groups with multiple members are the ‘Stephen’s Quintet’ and ‘Seyfert’s Sextet’, and the lesser known ‘Zwicky’s Triplet’ (Arp 103).

In the Uppsala General Catalogue, this multi-galactic system is confusingly listed as a single galaxy UGC 2489 (G1 in our nomenclature) positioned at $03^h01^m51.5^s$, $+35^d50^m30^s$ (Cotton et al. 1999). The SDSS optical and 2MASS near-IR images of the central region of Abell 407 are shown in Figs 1 and 2 (Left panel), and a zoomed ver-

sion is shown in Fig. 3 (Right panel), where we have also labeled the nine galactic condensations by letters G1 to G9 (see Table 1). The first column in Table 1 also gives Zwicky’s original nomenclature (within brackets) for these nine galaxies.

2.1 X-ray detection

The Abell 407 cluster is detected in the ROSAT All Sky Survey (RASS), with estimated X-ray luminosity and gas temperature of 5×10^{44} ergs $^{-1}$ (0.1-2.4 keV band) and 2.5 keV respectively (Ebeling et al. 1998). In MCXC (Meta Catalogue of X-ray Galaxy Clusters) it is listed as MCXC J0301.8+3550 (Piffaretti et al. 2011) with an estimated cluster mass $M_{500} = 9.16 \times 10^{13} M_{\odot}$, where M_{500} is the total mass enclosed inside a radius $R_{500} = 675.4$ kpc, within which the mean over-density of the cluster is 500 times the critical density at the cluster redshift. From archival X-ray data in RASS hard band (0.5 -2.4keV) we obtained surface brightness contours that are overlaid on GMRT 150 MHz image (Figure. 2; right panel). Here the projected separation of the optical center (taken as G1, the brightest member) and the brighter X-ray peak to the southwest is $\sim 1.7'$ or ~ 90 kpc. Similar offsets in the optical and X-ray emission peaks have been observed in systems with ongoing mergers or in dynamically active clusters (Rykoff et al. 2008; Mann & Ebeling 2012).

2.2 Previous radio observations of 4C 35.06

One of the earliest detections of this source is at 1.4 GHz frequency with the Cambridge one-mile telescope with fairly poor resolution (Riley 1975). Subsequently, this source has been studied using VLA at 1.4 GHz and 5 GHz by Bondi et al. (1993), revealing a bi-lobed structure at $\sim 5''$ resolution. At 1.4 GHz the total flux density of 4C 35.06 is 728 mJy, a core flux density of 10 mJy, an eastern lobe of 305 mJy, and a western lobe of 416 mJy. At 5 GHz, the total flux density was 170 mJy, with core flux of 4 mJy, an eastern lobe of 55 mJy and a western lobe of 114 mJy. A 5 GHz VLBA observation at 4.87×2.23 mas 2 resolution detected a compact radio core of 2.6 mJy peak flux (3.5 mJy integrated) associated with the galaxy G3, which is the second brightest member of the nonet (Liuzzo et al. 2010). However, the VLBA scale is only about 3 pc across, while the large-scale radio structure extends over 200 kpc, leaving a vast gap in our understanding of the connection between the compact AGN and larger radio morphology. Moreover, the previous high frequency VLA maps all miss the large-scale jet structure and ultra-steep spectrum outer regions of this source. Recently, using high resolution ($5''$ FWHM) and high sensitivity ($70 \mu\text{Jy}/\text{beam}$ rms) GMRT observations at 610 MHz frequency, Biju et al. (2014) drew attention to the complete radio structure of an unusual, helically twisted, kinked-jet system of the radio source 4C 35.06. Shulevski et al. (2015) have also studied this source at a very low radio frequency of 62 MHz with LOFAR at angular resolution of $50''$ FWHM. We discuss these observations along with our new GMRT observations in the sections below.

3 OBSERVATIONS AND DATA REDUCTION

3.1 Multi-wavelength GMRT radio observations

We observed 4C 35.06 with GMRT at three frequencies; 610, 235 and 150 MHz (Project codes 21_066 and 26_037 1). Table 2 shows the log of radio observations. For flux and bandpass calibrations, 3C 48 was observed at the beginning and end of the observation runs for 10 minutes. The 30-minute scans on target source were alternated by 5 minute scans on the phase calibrator. The data were reduced using NRAO AIPS software package. AIPS tasks SETJY and GETJY were used for flux density calibrations (Baars et al. 1977). The visibility data were flagged for Radio Frequency Interference (RFI) using AIPS tasks. The clean and calibrated solutions for the flux calibrator were used to calibrate the phase calibrator. The bandpass solutions were computed using the flux calibrator. These bandpass solutions were applied to the data and the frequency channels were averaged to increase the signal to noise ratio. The collapsed channel data were recalibrated for phase and amplitude solutions and later applied to the target source. AIPS task IMAGR was used for imaging in 3 dimensions, correcting for the W-term effects at low frequencies. For imaging, Briggs ROBUST weighting parameter was adjusted to detect low surface brightness diffuse emission regions better. Before the final imaging, several rounds of phase self-calibrations and one round of amplitude self-calibration were applied to the data. At 610 and 235 MHz, rms noise levels of $70 \mu\text{Jy}/\text{beam}$ and 0.90 mJy/beam were achieved, respectively. The rms noise measured in 150 MHz image was ~ 1 mJy/beam. In Fig. 4, the GMRT 610 MHz radio image of 4C 35.06 is shown overlaid on the SDSS i-band optical image.

From the VLA archives we also created high frequency radio maps using data in D and C scaled arrays, observed at 6cm (4.8 GHz) and 20cm (1.4 GHz) wavelengths, respectively. Standard routines in AIPS were used for calibration and imaging. For spectral index mapping, we imaged both data sets with identical $15''$ (FWHM) angular resolutions.

3.2 Spectroscopic Observations

We attempted to obtain good quality spectra for all nine galaxies comprising ‘Zwicky’s Nonet’. The optical spectroscopic observations of the brighter galaxy members G1, G3, G4, G7 and G9 were taken with the IUCAA Girawali Observatory (IGO) 2m telescope and fainter galaxies G2, G5 and G6 with the Palomar 200-inch telescope. The aim was to characterize their AGN and star forming activity, and to estimate the central velocity dispersions (σ) and black hole masses (M_{BH}) using the well known $M_{BH} - \sigma$ correlations (Gebhardt et al. 2000; Ferrarese & Merritt 2000).

Optical long-slit spectroscopic data were taken on 20-22 November 2011 on the IUCAA 2m telescope (IGO). The spectra were obtained using the IUCAA Faint Object Spectrograph and Camera (IFOSC) 2 . We used two IFOSC

¹ <https://naps.ncra.tifr.res.in/goa/mt/search/basicSearch>

² <http://igo.iucaa.in>

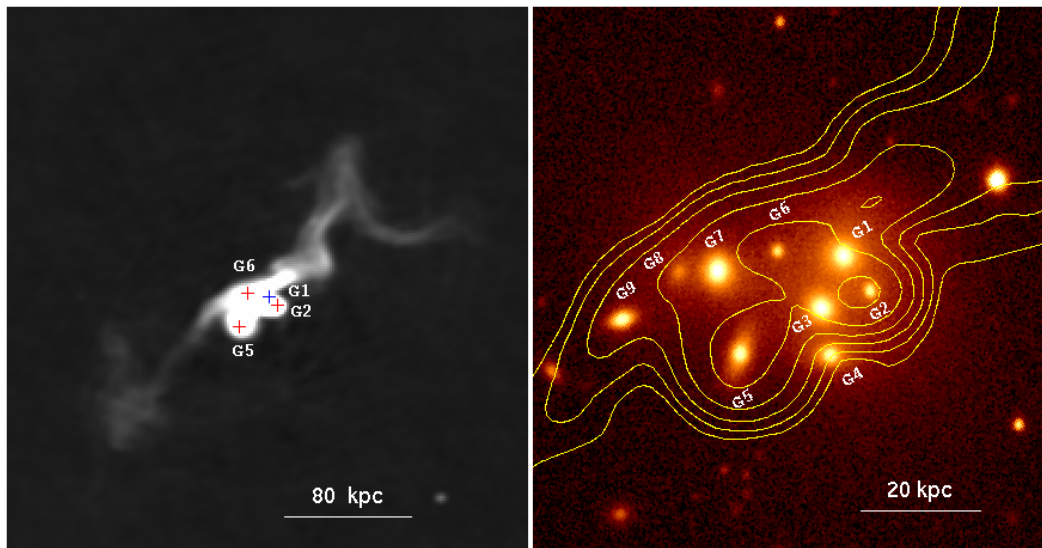


Figure 3. Left panel: 4C 35.06 at 610 MHz mapped ($5.8' \times 5.4'$) with GMRT at $5''$ resolution, with the positions of central galaxies G1 (the brightest member), and G2, G5 and G6 (possible radio sources) marked on it. Right panel: the SDSS zoomed i-band image ($1.4' \times 1.3'$) of the central region together with the GMRT 610 MHz radio contours plotted on it. In this figure, all the nine galaxies comprising ‘Zwicky’s Nonet’ have been marked. North is up, and east is to the left.

Table 2. Details of radio observations.

Telescope	Observed frequency	Band width	Obs. time	Beam (arc sec)	Map rms
GMRT	610 MHz	32 MHz	9hrs	5.83×4.78	0.07 mJy/b
GMRT	235 MHz	6 MHz	9hrs	20.86×16.68	0.9 mJy/b
GMRT	150 MHz	16 MHz	10hrs	19.87×15.77	1 mJy/b
VLA(NVSS) ^a	1.4 GHz	100 MHz	survey data	45×45	0.4 mJy/b
VLA(VLSS) ^b	74 MHz	1.56 MHz	survey data	80×80	100 mJy/b

^a (Condon et al. 1998) ^b (Cohen et al. 2007)

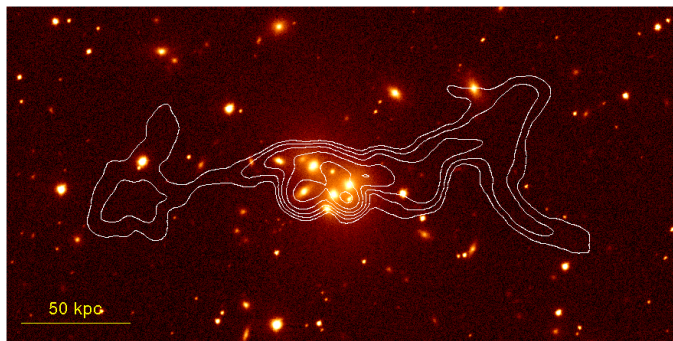


Figure 4. Optical i-band image ($5.7' \times 2.9'$) of the galaxy cluster Abell 407 taken from the Sloan Digital Sky Survey (SDSS). The white contours show the 610 MHz radio emission morphology of 4C 35.06 as imaged with GMRT at $5''$ resolution. Both the radio and optical images have been rotated for convenience.

grisms; grism no.7 and grism no.8 in combination with a 1.5-arcsec slit. These grisms provide a wavelength coverage of 3800-6840 Å and 5800-8350 Å. Standard stars were observed during the same nights for flux calibration. Wavelength calibration was done using standard Helium-Neon lamp spectra. Palomar 200-inch observations were carried out on 2014 Jan-

uary 23. The data were taken covering the wavelength range 3800 Å to 9500 Å, using the double spectrograph (blue and red arms). Wavelength calibration was done using standard Fe-Ar arc lamp spectra. Standard routines in the Image Reduction and Analysis Facility (IRAF) were used for data reduction and one-dimensional spectra were extracted using the *doslit* task in IRAF. The analysed data are added as supplementary material.

4 RESULTS AND DISCUSSION

4.1 The GMRT images of 4C 35.06: steep spectrum emission and source parameters

Figure 5 upper row presents the GMRT low frequency radio images at 610, 235 and 150 MHz. The regions marked A1, B1 and A2, B2 represent the features on jets while C denotes the core region. The regions D1 and D2 indicate the outermost diffuse structures of the source. The forthcoming sections give a detailed discussion of these regions. We also show the radio images from the NRAO VLA Sky Survey (NVSS, 1420 MHz) and VLA Low-frequency Sky Survey (VLSS, 74 MHz) in the bottom panel of Figure 5. The contours of the GMRT 150 MHz image are plotted over the NVSS and VLSS images

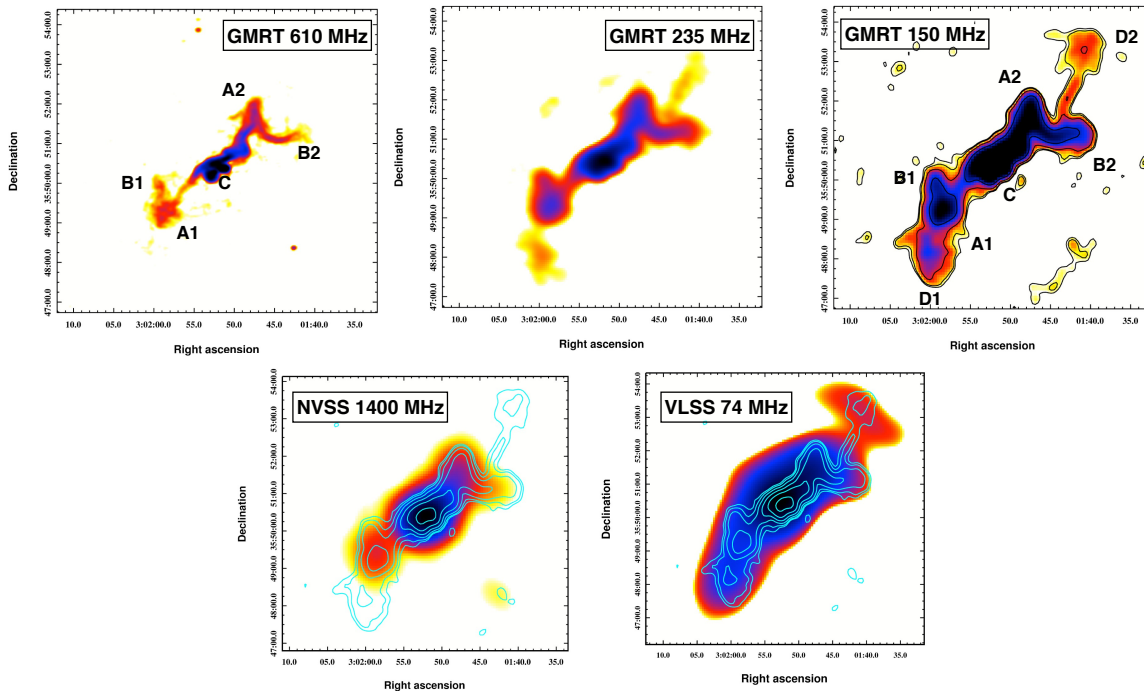


Figure 5. Colour scale GMRT images (Top Panel, left to right): at 610 MHz at resolution $5.83'' \times 4.78''$, 235 MHz at resolution $20.86'' \times 16.68''$, and 150 MHz (contour plot) with levels $[1, 2, 4, 8, 16, \dots] \times 4 \text{ mJy/beam}$ and resolution $23.9'' \times 19.36''$. Bottom Panel: Colour scale images showing 150 MHz GMRT contours plotted over 1400 MHz NVSS image (Bottom left) and 74 MHz VLSS image (Bottom right).

for size comparison. The highest resolution ($5''$ FWHM) and currently the deepest yet GMRT image at 610 MHz shows a bright, complex core region and associated double sided twisted/helical jet structure, while the NVSS 1.4 GHz image does not resolve these structures due to its poor resolution ($45''$ FWHM). The VLA 1.4 GHz image at $15''$ resolution detects the extended, twisting-turning jet structure (Fig. 5, bottom left panel). The low frequency 235 and 150 MHz GMRT maps show extended, steep spectrum ‘relic’ plasma emission features (see Figure 5) at the extremities of the helically twisted jet structure. These features were also detected in 62 MHz LOFAR map [Shulevski et al. (2015)].

At 610 MHz the source is found to have a total flux density of $1.7 \pm 0.12 \text{ Jy}$. The flux densities along the western and eastern jets are observed to be 580 mJy and 193 mJy respectively. The angular size of the source is $260''$ or linear size of $\sim 220 \text{ kpc}$. The maximum extent of the source at 235 MHz is $430''$ or $\sim 380 \text{ kpc}$. At 150 MHz the source is found to have the largest size of $460''$ or $\sim 400 \text{ kpc}$ linear size. This implies that the linear extent of the source grows larger with the lowering of frequency, which is suggestive of steep-spectrum emission regions present at the extremities. At these frequencies, the western jet is brighter than the eastern jet (2.37 Jy and 1.18 Jy at 150 MHz, and 1.72 Jy and 800 mJy at 235 MHz respectively). The total source flux densities at 150 MHz and 235 MHz are $6.0 \pm 0.18 \text{ Jy}$ and $4.7 \pm 0.13 \text{ Jy}$, respectively. The excellent quality GMRT images enabled us to make high resolution ($\sim 25''$) spectral index maps down to 150 MHz. These maps are discussed further in the following sections.

4.2 Where is the AGN radio core?

On the $5''$ resolution GMRT 610 MHz map of 4C 35.06, there are three radio peaks near the center, of which two are shifted south from the jet direction (Figure.3). A previous VLBA observation (Liuzzo et al. 2010) has detected a compact radio core in the galaxy G3 on parsec scale. The two GMRT 610 MHz radio peaks are centered near optical galaxies G5 and G2, while the third radio peak on the jet axis is close to the faint galaxy G6. Figure 3 (left panel) shows the positions of G2, G5, G6 and the brightest galaxy G1 with ‘+’ signs. Biju et al. (2014) suggested that the probable host AGN emitting the bipolar jet could be galaxy G6 rather than G3, which is clearly offset southward from the principal jet direction. The galaxy G6 is very faint both in optical and infrared light (Table 1 and 3). From spectroscopy, we obtained a velocity dispersion of $(143 \pm 40) \text{ Km s}^{-1}$ for G6, which yielded a relatively small black hole mass of $(0.52 \pm 0.65) \times 10^8 M_{\odot}$ (see section 4.7). However, the error margin is high due to the low SNR of the spectrum. Even though it is improbable (but not impossible) for a faint galaxy like G6 to produce such a large scale radio jet, it is possible that this now faint galaxy has been stripped off the majority of its outer halo stars in multiple tidal encounters, while still retaining a dense stellar core and black hole at the centre. Possibly this is also reflected in even smaller black hole mass, $(1.5 \pm 0.07) \times 10^7 M_{\odot}$ derived from its faint K-band luminosity of $M_K = -21.16$ (Table 3).

In an alternative scenario, Shulevski et al. (2015) have suggested that the rapid movement of galaxy G3 and its episodic AGN radio activity is the reason for the observed peculiar radio morphology of 4C 35.06. In their interpre-

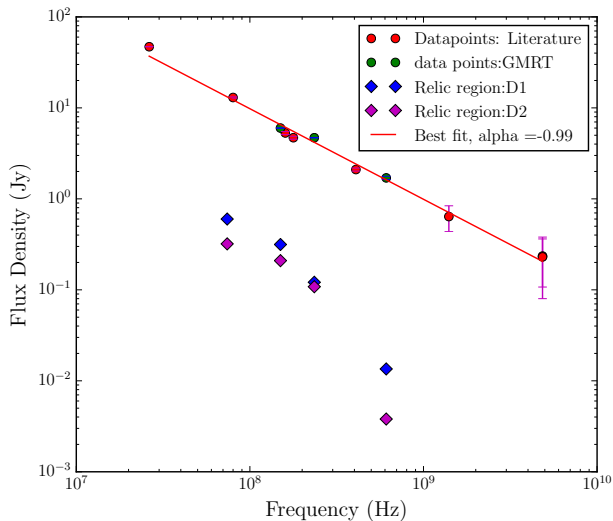


Figure 6. The integrated radio spectrum of 4C 35.06. A power law fit is shown by a red line. Red points are the data taken from literature and green points the GMRT observations. A pair of spectra shown with blue and pink data points represent the diffuse, relic regions D1 and D2 detected in GMRT low frequency images (Figure 5).

tation, the large scale jet morphology is due to the earlier phase of activity of G3, which had switched off its radio emission and then restarted while it was moving to its current position, resulting in the offset inner double-lobed morphology and steep-spectrum larger jet structure to the north, similar to dying radio galaxies (Murgia et al. 2011). Thus, at present, we are observing an aged FRI-like large scale structure with an embedded restarted radio source. Shulevski et al. (2015) also discuss that this AGN core is less likely to be G6 as argued by Biju et al. (2014), because of the lower mass of this galaxy and hence the lesser likelihood of it containing an SMBH. However, they have not considered the possibility of stripping of stars from the outer halo during tidal encounters in a dense environment, still retaining the SMBH at its center. In our opinion, the canonical black hole mass- IR bulge luminosity correlation applicable for normal ellipticals in relaxed environments may not hold good in the case of galaxies subjected to violent mergers. We suggest that the observation of the close coincidence of the optical positions of G2 and G5 with the radio peaks and the location of G6 near the center of symmetry of the large scale jets provide ample evidence to argue that the conclusion by Biju et al. (2014) might be justifiable. However, much higher resolution radio or X-ray data are still necessary to identify the compact AGN core and the progenitor galaxy of the large scale jet structure firmly.

4.3 Spectral Index Maps and Spectral Ageing Results

The integrated spectrum and spectral index maps are derived from the data available in the literature and our present GMRT observations. The broad-band spectrum shows an overall steep power-law from 26 MHz up to 4.9 GHz (Figure. 6). The GMRT data points clearly fit with the power-law spectral index $\alpha = -0.99$, thereby indicating

overall steep spectrum nature of the source, as compared to typical radio galaxies with jets and lobes.

To understand the energetics of this radio source better, we created spectral index maps at low and high frequency ends, using radio maps convolved to the same resolution. Figure 7 shows dual-frequency spectral index maps of the 235 vs. 610 MHz and 150 vs. 235 MHz bands. The spectral index maps clearly show that the radio emission in the central core region has flatter spectra in the range $\alpha = -0.5$ to -0.8 , whereas ultra-steep spectrum emission dominate at the outer extremities, with $\alpha \sim -2$ for 235-610 MHz and 150-235 MHz maps. The spectral indices for the diffuse, outermost relic regions marked D1 and D2 are estimated to be -1.79 and -2.10 respectively, indicating their ultra steep spectral nature (Figure 5 and 6). This suggests that the radio emission in region D1 and D2 originates from an ageing radio plasma subjected to heavy energy losses, possibly resulting from a previous phase of energy injection in the region. The LOFAR observations at 62 MHz (Shulevski et al. 2015) also detect these ultra-steep spectral regions, but less clearly in comparison with the higher sensitivity GMRT images. The central region shows a flat spectrum, possibly due to the superposition of emission from a few radio-loud AGNs, while the steep spectrum towards the extremities can be attributed to the lack of fresh injection of accelerated particles and radiative energy losses.

A high frequency spectral index map (Figure 8) was created by combining VLA D and C array maps at 6 cm (4.8 GHz) and 20 cm (1.4 GHz) wavelengths, both imaged at the same $15''$ angular resolution. This figure shows a flat spectral index central region with $\alpha \approx -0.5$ (dark shades) which steepens progressively away from the center along the twisting radio jets, with $\alpha > -2$ (light shades) at the extremities of the jets. Although the angular resolution of VLA maps is lower than that of GMRT, the spectral index trend is similar to that with GMRT maps.

The radiative age of the non-thermal plasma in regions D1 and D2 was obtained from the spectral breaks in the integrated radio spectra of the regions shown in Figure 9. The spectra are fitted with second order polynomials and tangents are drawn at 610 MHz and 150 MHz frequencies. The intersection point of these tangents gives the break frequency ν_b , obtained as 308 MHz and 302 MHz for regions D1 and D2 respectively. Beyond the breaks, a steepening or a possible cut-off in the spectra is suggested, consistent with the scenario of radio emission emanating from a rapidly cooling electron population.

The electron spectral age t_{sp} (or cooling time scale) is then estimated from the synchrotron radio spectrum using the formula (Murgia et al. 2011)

$$t_{sp} = 1.59 \times 10^9 \left[\frac{B^{1/2}}{[B^2 + B_{IC}^2] [\nu_b(1+z)]^{1/2}} \right] yr \quad (1)$$

This formula is obtained for a uniform magnetic field, neglecting expansion losses over the radiative age. Here B is the magnetic field in μG , z is the redshift, $B_{IC} = 3.25(1+z)^2 \mu\text{G}$ is the inverse Compton equivalent magnetic field and ν_b is the cooling break frequency in GHz. An independent estimate of the magnetic field in the relic regions is needed for a robust estimate of t_{sp} .

Assuming minimum energy condition, we calculated the

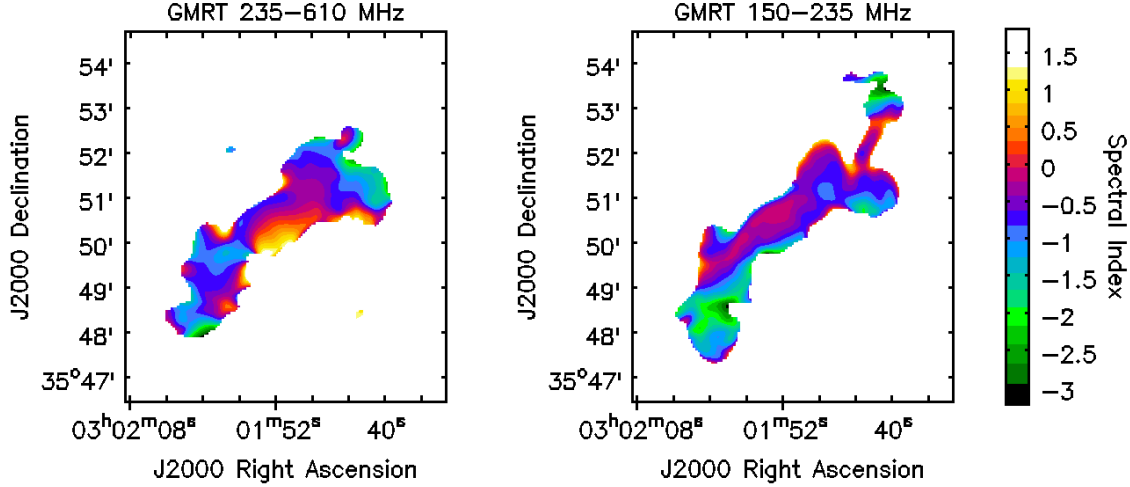


Figure 7. The spectral index maps obtained from 235 MHz vs. 610 MHz (left panel) and 235 MHz vs. 150 MHz GMRT images (right panel) using matched resolutions. The spectral index values are shown with a color bar on the right edge. In both plots, the spectral index errors in the central region (~ 0.02 and ~ 0.1) are much lower than that near the jet extremities (~ 0.2 and ~ 1).

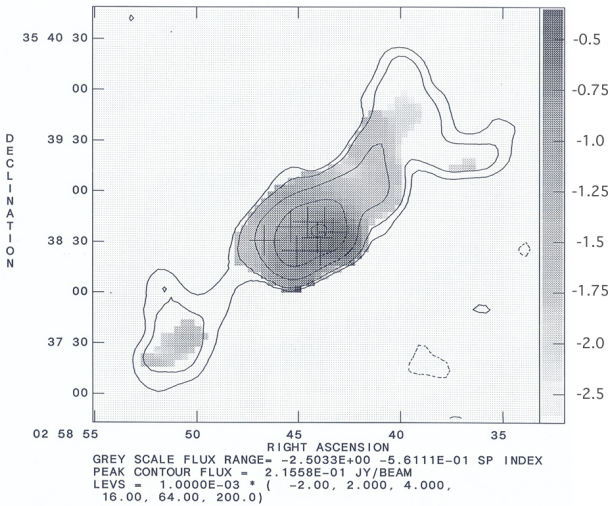


Figure 8. The spectral index map of 4C 35.06 shown in grayscale, obtained by combining D and C scaled-array VLA data at 6cm and 20cm wavelengths at $15''$ resolution. The contours are the VLA 20cm (1.4 GHz) radio contours at the same resolution, and contour levels in mJy/beam are shown at the bottom of the image. The optical galaxies in the center are denoted with '+' symbols.

energy density and magnetic field in the regions A1, A2 (the inner loop structures), and D1, D2 (the outer relic regions) (see Figure 5). The minimum energy density u_{min} is given by:

$$u_{min} = \xi(\alpha, \nu_1, \nu_2)(1+k)^{4/7}(\nu_o)^{4\alpha/7}(1+z)^{(12+4\alpha)/7}(I_o/d)^{4/7} \quad (2)$$

where k is the ratio of the energy of the relativistic protons to that of electrons, α is the spectral index, ν_1 and ν_2 are lower and higher limits of frequency, ν_o is the frequency at which surface brightness I_o is measured, and function $\xi(\alpha, \nu_1, \nu_2)$ is tabulated in Govoni & Feretti (2004). Here we assume the filling factor to be 1, $\nu_1 = 10$ MHz, $\nu_2 = 10$ GHz, $\nu_o = 150$ MHz and $z = 0.047$.

The equipartition magnetic field can be expressed by:

$$B_{eq} = \left(\frac{24\pi}{7} u_{min}\right)^{1/2} \quad (3)$$

This way the magnetic fields for the relic regions are obtained as $\approx 5\mu\text{G}$ and $\approx 16\mu\text{G}$ for $k = 1$ and $k = 100$, respectively. The corresponding elapsed times are ~ 170 and ~ 40 Myr, respectively.

We point out that Shulevski et al. (2015) calculated the spectral age by estimating the time taken by the galaxy G3 (putative central AGN) to translate from the former location (at the center of the east-west jet direction), by approximating the radial velocity difference between the galaxy and the stellar envelope (Schneider & Gunn 1982) as the velocity of the source in the sky plane. It was assumed that the source was shut off before the translation and restarted once it reached the new position. This approximation enabled them to adopt the translation time of G3 to be the shutdown period (t_{off}) of the AGN. An estimate of spectral age was made assuming equal time scales for active (t_{on}) and quiescent (t_{off}) phases of the AGN and adjudging the sum ($t_{on} + t_{off}$) = 70 Myrs as the age of the radio plasma. Assuming lowest the Lorentz factor values, they obtained a magnetic field of $10\mu\text{G}$ and a corresponding break frequency of ~ 380 MHz, which is very close to the break frequency (~ 300 MHz) we obtained from the GMRT data points. Even though the restarted AGN activity model and the present model yield almost same values for break frequency, many assumptions had to be invoked to substantiate the former model.

4.4 Twists and kinks in the jet: Dynamical signatures of a perturbed AGN ?

The GMRT 610 MHz maps (Figures 3 and 5) reveal that the bipolar radio jet undergoes helical twists, with inversion symmetry, on either side of core C at the points marked A1

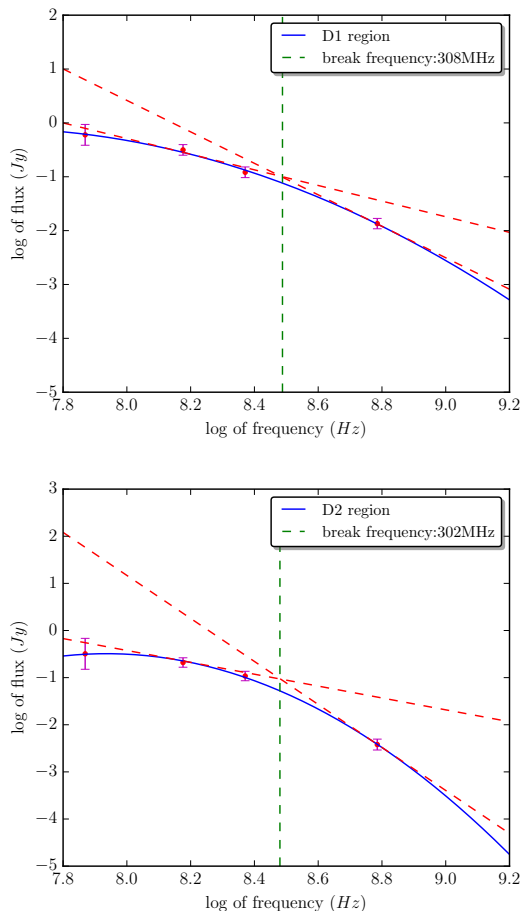


Figure 9. The second order polynomial spectral fit (blue line) for the outermost regions D1 (Top panel) and D2 (bottom panel). The flux values are taken at frequencies 610, 235, 150 (GMRT) and 74 MHz (VLASS). The dashed red lines represent the tangents drawn at higher (610 MHz) and lower frequency (150 MHz) ends of spectra and the intersection point denotes the estimated break frequency (green dotted line).

and A2 in Figures. 5 and 10. Moreover, the north-west arm of the jet is observed to be brighter, and bends to form a prominent loop/arc starting from A2 up to point B2. A similarly twisted feature between points A1 and B1 is observed in the south-east arm as well, but fainter and more diffuse compared with the north-western counterpart.

The region D2 in the western arm shows a peculiar, upward bent jet-like structure in the 150 MHz GMRT map, capped by a ‘mushroom’ like feature at the top, the nature of which is not clear at the moment (Figure. 5 upper panel). The symmetric counterpart of this knot/mushroom structure could be the downward bent feature D1 in the south-eastern section of the source. The extremely steep high-frequency radio spectra of the mushroom like feature at D2 (and also D1), located ~ 200 kpc from the center, indicate significant energy losses, suggesting an absence of freshly injected particles. One possibility is that they are buoyant non-thermal plasma bubbles rising into the hot intra-cluster medium, inflated by the radio jet in the past, as observed around some BCG/cD galaxies residing in centers of clusters or groups (Bagchi et al. 2009; McNamara & Nulsen 2012).

In addition to these interesting features there are a few

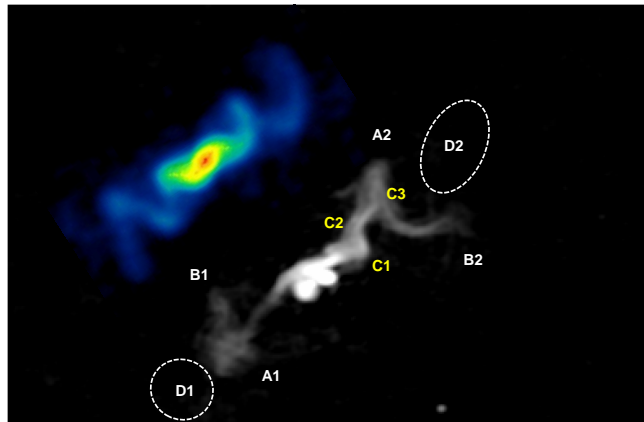


Figure 10. The high resolution ($5''$) grayscale image of the source 4C 35.06 at 610 MHz (GMRT) showing the twisted, helical jet structure. Different regions of the source are marked, and the end extensions D1 and D2 detected at 235 MHz and 150 MHz, are indicated by dotted lines. The colour image shows, for comparison, the cork-screw shaped precessing jets observed in galactic XRB ‘microquasar’ SS433, which is the total intensity image at 4.85 GHz (Blundell & Bowler 2004). Note the linear size of SS 433 jet system is only 0.26 pc while that of 4C 35.06 at 610 MHz is 230 kpc.

sharp kinks or steps in the western arm of the jet at points marked C1, C2 and C3 (Figure. 10). On the eastern side of the jet these kinks/steps are not discernible, possibly due to the projection effects or their absence. In our present work, lacking detailed modeling, it is difficult to decipher what these kinks in the jet flow represent physically, but they have been discussed further below (in Section 4.5 & 4.6).

4.5 Precessing radio jet structure: comparison with galactic microquasar SS 433

The deciphering of the peculiar radio jet morphology of 4C 35.06 gains added impetus when it is compared with a precessing radio jet structure observed in the galactic ‘microquasar’ SS 433 (see Figure 10). SS 433 is an X-ray binary (XRB) system in the center of supernova remnant W50, consisting of a stellar mass black hole or neutron star accreting matter from an A-type supergiant donor star (Milgrom 1979; Abell & Margon 1979; Blundell & Bowler 2004). The most unusual aspect of this object, modelled through radial velocity measurements of ‘shifting’ H_{α} lines and high resolution radio imaging, is that the accretion disk around the compact object precesses with a regular period of ~ 164 days (Milgrom 1979; Abell & Margon 1979). Consequently, the axis of the jet-ejection nozzle also precesses with the same period and the ejected radio plasma traces out a dynamically changing ‘corkscrew’ pattern (see Figure 10 and Blundell & Bowler (2004)).

Even though a detailed modelling of the precession geometry of 4C 35.06 is beyond the scope of the present study, it is noticeable that its large-scale jet structure is analogous to that of SS 433, if we ignore the kinks (C1, C2 and C3) for the time being. The loop portions A2 - B2 and A1 - B1 are suggestive of the corkscrew pattern resulting from con-

tinuous change of the jet axis, possibly due to a precessing motion. Further, flat spectrum terminal hot spots are absent at the jet extremities of 4C 35.06 as well as SS 433, which is another indication of the continuous shifting of the jet direction.

Moreover, the brightness of the western arm of the jet system in 4C 35.06 is nearly double that of the eastern arm. Depending on the inclination of the jet axis with our line of sight, the precession cone angle and the plasma bulk velocity, the projected radio morphology and brightness can appear to be quite different on the approaching and receding sides. This has been shown by Gower et al. (1982) in numerical simulation of relativistic effects in precessing jets. The differences in the observed jet morphology on the two sides can be attributed as partly due to this.

The precession of radio jets may be attributable to two mechanisms: first, the presence of a binary black hole system (Begelman et al. 1980; Deane et al. 2014), where the torque exerted by the companion black hole can precess the accretion disk of the first object, leading to jet precession and secondly, the Lense-Thirring frame dragging effect (Bardeen & Petterson 1975); if the angular momentum vector of the accretion disk is misaligned with that of a fast spinning Kerr black hole, the black hole will try to frame drag the inner accretion disk so as to align it with its spin vector. This will lead to the precession of the accretion disk and of radio jets orthogonal to it. If this is the reason for the helically twisted jets in 4C 35.06, an interesting corollary is that the mass accreting supermassive black hole must be spinning. Moreover, the observed resemblance of the morphology of 4C 35.06 to the precessing relativistic jet system of X-ray binary SS 433 supports the fundamental paradigm that, in spite of a vast difference in involved black hole masses, length and time-scales, almost all relativistic disk-jet coupled phenomena happen in a scale-invariant manner in radio-loud AGNs and the galactic microquasars.

4.6 Jet energetics and interaction of jets with the ambient intracluster medium

In Figure 2 (right panel), the GMRT 150 MHz radio image of 4C 35.06 is shown superposed on the ROSAT X-ray map in the 0.5 - 2.4 keV band. Here we observe that the energetic jet system of 4C 35.06 has expanded preferentially in the direction of lower gas pressure in the dense intra-cluster medium. This might affect the ambient X-ray medium by uplifting the gas along the mean jet flow direction. This radio jet feedback effect could be analogous to the distorted, extended lobes of supernova remnant W50 (the ‘Manatee’ nebula), which are shaped by the interaction of powerful jets in microquasar SS 433 with the ambient ISM (Dubner et al. 1998). We need much deeper X-ray observations of the A407 cluster to investigate the AGN feedback signatures better.

Observationally, the kinetic power of a jet (\dot{Q}) is a key descriptor of the state of an accreting SMBH system: its mass, spin and the magnetic field of the accretion disk. Correlation of low-frequency ($\nu \sim 150$ MHz) radiative power of radio sources against their jet power shows that the radio luminosity of the jet constitutes only a small fraction ($< 1\%$) of the total kinetic power (Punsly 2005; Daly et al. 2012). Using the 150 MHz radio flux density of 6.0 ± 0.18 Jy from the GMRT map, the time averaged kinetic power of jets in

4C 35.06 is computed as $\bar{Q} \approx 3 \times 10^{43} \text{ erg s}^{-1}$ (Punsly 2005). We have not corrected for the (unknown) loss of energy in the outer radio lobes and thus \bar{Q} is likely to be a lower limit. This power is below the transition value $5.0 \times 10^{43} \text{ erg s}^{-1}$ between FR I and II classes. However, if the jet continues to operate between $10^7 - 10^8$ yr, the injected mechanical energy is $\sim 10^{58} - 10^{59} \text{ erg}$, which is large enough to affect or even quench any cooling flow strongly and to drive large-scale outflows that redistribute and heat the gas on cluster-wide scales. If we further assume that this jet power is derived from accretion flow onto a black hole at the rate \dot{M} and $\bar{Q} \sim 0.1 \dot{M} c^2$, we obtain $\dot{M} \sim 5.3 \times 10^{-3} M_{\odot} \text{ yr}^{-1}$. This number is only representative, but it suggests accretion at sub-Eddington rate $\lambda = \bar{Q}/L_{\text{edd}} = 0.0024 \times (10^8/M_{BH})$, where L_{edd} is eddington luminosity and M_{BH} is the mass of the black hole. This low accretion rate signifies a radiatively inefficient accretion flow (RIAF) in a low-luminosity active galactic nuclei (so called LLAGN or LINER). The optical spectra of the galaxies in Zwicky’s Nonet (refer Section. 4.7) also confirms this nature. However a complete picture of the launch of radio jet in 4C 35.06 and its energetic feedback effects requires much deeper and higher resolution X-ray and radio data.

Systems hosting helically modulated symmetric jets are the most promising sites for finding close black hole systems (triple or binary) (Deane et al. 2014; Begelman et al. 1980). In Zwicky’s Nonet, it is observed that seven galaxy pairs are separated by distances ~ 10 kpc in projection. Their redshift values are also close, with a mean $\bar{z} = 0.0469$ and standard deviation $\sigma_z = 0.00176$, or $v \sim 520 \text{ km s}^{-1}$ (refer Table 1). The number of binary or triple black hole systems discovered with projected separations less than a few kpc are very low (Deane et al. 2014). In the present dense system of nine galaxies, all packed within a radius of only 25 kpc, the smallest projected separation between galaxy pair combinations is about 5 kpc (between G7 and G8). So the extreme closeness of the galactic members coupled with the helically twisted, large scale jet structure highlights the prime importance of this galaxy group in the search of multiple supermassive black hole systems and their gravitational and electromagnetic merger signatures. Moreover, merging SMBHs would also lead to an enhanced rate of tidal disruption of stars and possible gravitational wave recoil (slingshot) ejection of black holes from galaxies at speeds in excess of 1000 km s^{-1} . Even though the symmetric helical pattern observed in the jet structure might be explained with precession model, there are a few anomalies like the presence of distinct kinks or steps denoted by C1, C2 and C3 in the north-western arm that pose a challenge. The precession model alone may be insufficient to explain these features. We note that C-shaped twisted paired jet system in radio source 3C 75 is associated with a binary black hole pair separated by only 7 kpc (Owen et al. 1985). Both the jets in 3C 75 show prominent wiggled and kinked structures, which have been modelled as due to the combined linear and orbital motion of the bound binary black hole pair (Yokosawa & Inoue 1985). In 4C 35.05 observed kinks could arise from a similar system, where a black hole with radio jets is orbiting another one at high speed and with large orbital eccentricity (Yokosawa & Inoue 1985). However, in this model, we can not easily explain why these kinks or steps are absent in the south-eastern arm of the jet.

Table 3. K band absolute magnitudes and masses of the SMBHs associated with the nine galaxies of ‘Zwicky’s Nonet’.

Source	K Band absolute magnitude	Mass of the SMBH. ($10^8 M_\odot$)
G1	-23.46±0.039	1.13 ±0.30
G2	-21.99±0.085	0.31±0.12
G3	-23.49±0.034	1.16±0.30
G4	-22.60±0.028	0.53±0.17
G5	-22.73±0.031	0.60±0.18
G6	-21.16±0.089	0.15±0.07
G7	-23.56±0.031	1.23±0.30
G8	-20.06±0.113	0.06±0.03
G9	-22.50±0.039	0.49±0.16

4.7 Optical spectroscopic results: AGN signature and black hole mass estimation

Previously, Schneider & Gunn (1982) measured the redshifts and stellar velocity dispersions (σ) for a few of galaxies in Zwicky’s nonet covering a wavelength range from 3700 to 5250Å. In our present study, we have obtained good S/N spectra over the wavelength range of 3800 to 8500Å for eight out of the nine galaxies comprising Zwicky’s Nonet (The spectra are included as supplementary material). However, attempt to obtain a fair spectrum of galaxy G8 failed, due to it being very faint. Our main aim was to search for the signs of AGN or star forming activity in the optical spectra of these galaxies and to estimate their black hole masses from the stellar velocity dispersion. The spectra of these galaxies resemble those of passive, early type red ellipticals, devoid of any major emission lines. This is not unusual as optical emission lines are found to be absent in many AGNs showing radio emission and large scale radio jets. It has been observed that many FRI radio sources in galaxy clusters are hosted by galaxies showing very weak or no optical emission lines (Zirbel & Baum 1995; Best & Heckman 2012).

Internal properties of a galaxy, such as mass and accretion rate of a SMBH are better estimated from the nuclear emission lines (Kauffmann et al. 2008). The observed spectra show that all the suspected radio loud galaxies (G2, G3, G5 and G6) belong to the class of low excitation radio galaxies (LERGs) (Lin et al. 2010; Hardcastle et al. 2006). LERGs are mostly found to be hosted by BCGs having extended cD like light profiles (Best & Heckman 2012), similar to what we find in Zwicky’s Nonet.

The well-known tight correlation which connects the mass of the central black hole M_{BH} to the galaxy’s bulge stellar velocity dispersion σ (Gebhardt et al. 2000; Ferrarese & Merritt 2000) is given by

$$\log_{10} \left(\frac{M_{BH}}{M_\odot} \right) = \alpha + \beta \log_{10} \left(\frac{\sigma}{200 \text{ km s}^{-1}} \right) \quad (4)$$

where σ is expressed in km s^{-1} . Here we have used $\alpha = 8.38$ and $\beta = 4.53$, as derived in McConnell et al. (2011). The estimated SMBH masses are tabulated in Table 4. The black hole masses were also calculated using the slightly different α and β values taken from Gültekin et al. (2009) and

McConnell & Ma (2013). These masses are consistent within one sigma limits with the numbers given in Table 4. These results show that galaxies G1, G3, G5, G7, and G9 all host supermassive black holes of mass ($M_{BH} \approx few \times 10^8 M_\odot$). For the other three galaxies G2, G4 and G6, the estimate of M_{BH} has large errors. Interestingly, the most massive black hole of mass $M_{BH} \approx 10^9 M_\odot$ resides in the galaxy G3, which showed a radio loud AGN core in previous VLBA observations (Liuzzo et al. 2010).

The galaxy black hole masses are also calculated from their K-band magnitudes using 6 times deeper data on cluster A407 available from 2MASS survey. The equation connecting K-band absolute magnitude (M_K), of bulge component to the central black hole mass given by Graham (2007) is,

$$\log_{10} \left(\frac{M_{BH}}{M_\odot} \right) = -0.38(\pm 0.06) (M_K + 24) + 8.26(\pm 0.11) \quad (5)$$

Table 3 lists the black hole masses estimated with this method for the nine galaxies. The following caveats are worth mentioning here: It is unclear whether the canonical M_{BH} - σ relation will suffice for galaxies in such a hostile environment, undergoing violent mergers and stripping of stars in multiple tidal encounters. This is clearly evidenced by the formation of a large-scale stellar halo of stripped matter in Zwicky’s Nonet. The same concern applies if one were to obtain M_{BH} from the K-band magnitude of bulge using the M_{BH} - M_K correlation. Moreover, effect of the gravitational potential of the background stellar halo (which is highly dark matter dominated; (Schneider & Gunn 1982)) and close merging galaxies on the bulge stellar velocity dispersion of a galaxy are also possible factors that need to be accounted for in black hole mass calculations. In this article, we have not attempted to do so. However, for checking this issue, the last column of Table 4 shows the ratio of black hole mass, from the M_{BH} - σ correlation ($M_{BH,\sigma}$) to that obtained from M_{BH} - M_K method ($M_{BH,K}$). The ratio $M_{BH,\sigma}/M_{BH,K}$ is > 2 for galaxies with well determined black hole masses, which suggests that possibly M_{BH} - M_K method gives smaller black hole masses because of the truncation of the outer envelope of galaxies, which reduces their K-band luminosity. Alternatively, the black hole masses from the M_{BH} - σ relation are overestimated.

The stripped away matter from the presently observed nuclei must provide a large fraction of the total luminosity of the observed stellar halo. The main parameters of the stellar halo, which is detectable up to the r-band surface brightness limit of $\sim 24 \text{ mag arcsec}^{-2}$ (and possibly beyond), quoted by Schneider & Gunn (1982) are as follows; central mass density $\rho(0) = 0.63 \pm 0.25 M_\odot \text{ pc}^{-3}$, mass-to-light ratio in r band $M/L = 90 \pm 35$, and halo radial velocity dispersion $\sigma_{halo} = 610 \pm 200 \text{ km s}^{-1}$. From this value of σ_{halo} and taking halo radius $r \approx 30''$ ($\sim 26.5 \text{ kpc}$), we obtain the total dynamical mass of halo as $2.2 \times 10^{12} M_\odot$, which interestingly is of the same order as that of a super giant cD galaxy.

Table 4. The redshifts and masses of the SMBHs associated with the galaxy like condensations in ‘Zwicky’s Nonet’. The last column shows the ratio of the SMBH black hole masses obtained from stellar velocity dispersions and K band magnitudes.

Galaxy	Red shift	Velocity dispersion (kms^{-1})	Mass of the SMBH ($10^8 M_{\odot}$)	SMBH mass ratio $M_{BH,\sigma}/M_{BH,K}$
G1	0.0473	222 ±16	3.88± 1.23	2.76
G2	0.0476	143 ±27	0.53 ± 0.44	1.71
G3	0.0470	273±18	9.83 ± 2.96	8.47
G4	0.0503	135±33	0.40 ± 0.45	0.76
G5	0.0476	230±8	4.52± 0.74	7.5
G6	0.0454	143±40	0.52± 0.65	3.47
G7	0.0468	211±16	3.08±1.00	2.50
G9	0.0445	176±20	1.34±0.68	2.74

5 CONCLUSIONS

We have presented the results of our radio, optical and infrared observations of the radio source 4C 35.06, located in the central region of the galaxy cluster Abell 407. The cluster center hosts a compact ensemble of nine passive, red elliptical galaxies embedded within a faint, diffuse stellar halo. We proposed to name this galactic system ‘Zwicky’s Nonet’.

GMRT observations at 150, 235 and 610 MHz clearly reveal the complete radio structure of 4C 35.06, with a complex central core region and helically twisted and kinked bipolar radio jets extending up to ~ 400 kpc. The radio jets terminate into diffuse, ultra-steep spectrum ‘relic/fossil’ plasma lobes D1 and D2. In D2, a peculiar, very steep spectrum ($\alpha < -2$) mushroom like feature is discovered from GMRT 150 MHz map.

In regions D1 and D2 of 4C 35.06, the average minimum energy magnetic field is $B \sim 5 \mu G$ for $k = 1$ and $B \sim 16 \mu G$ for $k = 100$. The corresponding spectral ages of electrons are obtained as 170×10^6 and 40×10^6 yr respectively. The time averaged kinetic power of jets is estimated to be $\approx 3 \times 10^{43} \text{erg s}^{-1}$, indicating that the source is a FR I type radio galaxy.

The unique helical jet system and the very compact configuration of nine galactic nuclei point to the possibility of precessional and orbital motion of the AGN. This also suggests possible gravitational perturbation effects of multiple black holes residing in the extremely dense central region of the cluster. In such an environment, orbital decay assisted by dynamical friction causes the central binary black holes of galaxies to merge, while gravitational torque in the binary phase may cause the accretion disk of AGN to precess, resulting in a helical jet pattern.

The morphological similarity of this jet system with that of the galactic microquasar SS 433 also supports a precessional scenario. The absence of terminal hot spots and presence of ultra-steep spectrum regions on both ends of the jet strongly suggest the continuous shifting of the jet direction, further supporting the precessional model.

Our study points to the possibility of the fainter member (G6) of the Zwicky’s Nonet hosting large-scale radio jets. The faintness of this galaxy is attributed to the stripping of its major stellar envelope due to the tidal interactions in galactic mergers, retaining the SMBH at the center. The high ratio (> 2) of black hole masses from stellar veloc-

ity dispersion and K-band luminosity, i.e. $M_{BH,\sigma}/M_{BH,K}$, for galaxies with well determined black hole masses corroborates the diminution of the stellar envelope. The observation of a diffuse stellar halo of stripped matter in the system supports this scenario.

The optical spectra of eight galaxies in Zwicky’s Nonet fail to show any prominent emission lines, indicating a radiatively inefficient accretion flow onto the central black holes at sub-Eddington rates. No strong star-formation/star-burst activity detected in any of the galaxy spectra.

Further high sensitivity and higher resolution radio observations are needed to provide a complete spectral analysis and to obtain the detailed resolved central morphology of this complex source. A deep X-ray observation of the hot intra-cluster gas around the cD galaxy precursor, and detection of the AGNs and their X-ray spectra would be very beneficial in deciphering the nature of this puzzling radio galaxy.

ACKNOWLEDGMENTS

We thank the staff of GMRT, IUCAA/IGO and Palomar Observatory for their help during the observations. GMRT is run by the National Centre for Radio Astrophysics of the Tata Institute of Fundamental Research. JB, JJ and PD acknowledge generous support from the Indo-French Center for the Promotion of Advanced Research (Centre Franco-Indien pour la Promotion de la Recherche Avancée) under programme no. 5204-2. KGB and JJ acknowledge IUCAAs support under the Visiting Associate program. KGB gratefully acknowledges the support received through Faculty Development Programme of the UGC, India. AAM and SGD acknowledge partial support from the NSF grants AST-1413600 and AST-1518308. MBP gratefully acknowledges support by DST INSPIRE Faculty Scheme, New Delhi. We have used images and results from SDSS and funding for SDSS has been provided by the Alfred P. Sloan Foundation, the participating institutions, the National Science Foundation, and the U.S. Department of Energy’s Office of Science. This research has made use of the NASA/IPAC Extragalactic Database (NED) which is operated by the Jet Propulsion Laboratory, California Institute of Technology, under contract with the NASA. We have used VLA data. The VLA is a facility of the National Radio Astronomy Observatory (NRAO).

REFERENCES

- Abell G. O., Corwin, Jr. H. G., Olowin R. P., 1989, ApJS, 70, 1
- Abell G. O., Margon B., 1979, Nature, 279, 701
- Baars J. W. M., Genzel R., Pauliny-Toth I. I. K., Witzel A., 1977, A&A, 61, 99
- Bagchi J., Jacob J., Gopal-Krishna, Werner N., Wadnerkar N., Belapure J., Kumbharkhane A. C., 2009, MNRAS, 399, 601
- Bagchi J., Kapahi V. K., 1994, Journal of Astrophysics and Astronomy, 15, 275
- Bardeen J. M., Petterson J. A., 1975, ApJ, 195, L65

- Begelman M. C., Blandford R. D., Rees M. J., 1980, *Nature*, 287, 307
- Best P. N., Heckman T. M., 2012, *MNRAS*, 421, 1569
- Biju K. G., Pandey-Pommier M., Sunilkumar P., Dhurde S., Bagchi J., Ishwara-Chandra C. H., Jacob J., 2014, in *Astronomical Society of India Conference Series (Metre Wavelength Sky Conference, Pune, India)*, Vol. 13, pp. 155–156
- Blundell K. M., Bowler M. G., 2004, *ApJ*, 616, L159
- Bondi M., Gregorini L., Padrielli L., Parma P., 1993, *A&AS*, 101, 431
- Cohen A. S., Lane W. M., Cotton W. D., Kassim N. E., Lazio T. J. W., Perley R. A., Condon J. J., Erickson W. C., 2007, *AJ*, 134, 1245
- Condon J. J., Cotton W. D., Greisen E. W., Yin Q. F., Perley R. A., Taylor G. B., Broderick J. J., 1998, *AJ*, 115, 1693
- Cotton W. D., Condon J. J., Arbizzani E., 1999, *ApJS*, 125, 409
- Daly R. A., Sprinkle T. B., O’Dea C. P., Kharb P., Baum S. A., 2012, *MNRAS*, 423, 2498
- Deane R. P. et al., 2014, *Nature*, 511, 57
- Dubner G. M., Holdaway M., Goss W. M., Mirabel I. F., 1998, *AJ*, 116, 1842
- Ebeling H., Edge A. C., Bohringer H., Allen S. W., Crawford C. S., Fabian A. C., Voges W., Huchra J. P., 1998, *MNRAS*, 301, 881
- Ferrarese L., Merritt D., 2000, *ApJ*, 539, L9
- Garijo A., Athanassoula E., Garcia-Gomez C., 1997, *A&A*, 327, 930
- Gebhardt K. et al., 2000, *ApJ*, 539, L13
- Govoni F., Feretti L., 2004, *International Journal of Modern Physics D*, 13, 1549
- Gower A. C., Gregory P. C., Unruh W. G., Hutchings J. B., 1982, *ApJ*, 262, 478
- Graham A. W., 2007, *MNRAS*, 379, 711
- Guidetti D., Murgia M., Govoni F., Parma P., Gregorini L., de Ruiter H. R., Cameron R. A., Fanti R., 2008, *A&A*, 483, 699
- Gültekin K. et al., 2009, *ApJ*, 698, 198
- Hardcastle M. J., Evans D. A., Croston J. H., 2006, *MNRAS*, 370, 1893
- Janiuk A., Proga D., Kurosawa R., 2008, *ApJ*, 681, 58
- Kauffmann G., Heckman T. M., Best P. N., 2008, *MNRAS*, 384, 953
- Kulkarni G., Loeb A., 2012, *MNRAS*, 422, 1306
- Lin Y.-T., Shen Y., Strauss M. A., Richards G. T., Lunnan R., 2010, *ApJ*, 723, 1119
- Liuzzo E., Giovannini G., Giroletti M., Taylor G. B., 2010, *A&A*, 516, A1
- Lu J. F., 1990, *A&A*, 229, 424
- Mann A. W., Ebeling H., 2012, *MNRAS*, 420, 2120
- McConnell N. J., Ma C.-P., 2013, *ApJ*, 764, 184
- McConnell N. J., Ma C.-P., Gebhardt K., Wright S. A., Murphy J. D., Lauer T. R., Graham J. R., Richstone D. O., 2011, *Nature*, 480, 215
- McNamara B. R., Nulsen P. E. J., 2007, *ARA&A*, 45, 117
- McNamara B. R., Nulsen P. E. J., 2012, *New Journal of Physics*, 14, 055023
- Milgrom M., 1979, *A&A*, 76, L3
- Murgia M. et al., 2011, *A&A*, 526, A148
- Owen F. N., O’Dea C. P., Inoue M., Eilek J. A., 1985, *ApJ*, 294, L85
- Paul S., Iapichino L., Miniati F., Bagchi J., Mannheim K., 2011, *ApJ*, 726, 17
- Piffaretti R., Arnaud M., Pratt G. W., Pointecouteau E., Melin J.-B., 2011, *A&A*, 534, A109
- Punsly B., 2005, *ApJ*, 623, L9
- Riley J. M., 1975, *MNRAS*, 170, 53
- Rykoff E. S. et al., 2008, *ApJ*, 675, 1106
- Schneider D. P., Gunn J. E., 1982, *ApJ*, 263, 14
- Shulevski A. et al., 2015, *A&A*, 579, A27
- Subramanian K., Shukurov A., Haugen N. E. L., 2006, *MNRAS*, 366, 1437
- Tovmassian H. M., Andernach H., 2012, *MNRAS*, 427, 2047
- Volonteri M., Haardt F., Madau P., 2003, *ApJ*, 582, 559
- Wilson A. S., Colbert E. J. M., 1995, *ApJ*, 438, 62
- Wright E. L., 2006, *PASP*, 118, 1711
- Yokosawa M., Inoue M., 1985, *PASJ*, 37, 655
- Zirbel E. L., Baum S. A., 1995, *ApJ*, 448, 521
- Zwicky F., Zwicky M. A., 1971, *Catalogue of selected compact galaxies and of post-eruptive galaxies (Switzerland: Guemligen)*

SUPPLEMENTARY MATERIAL

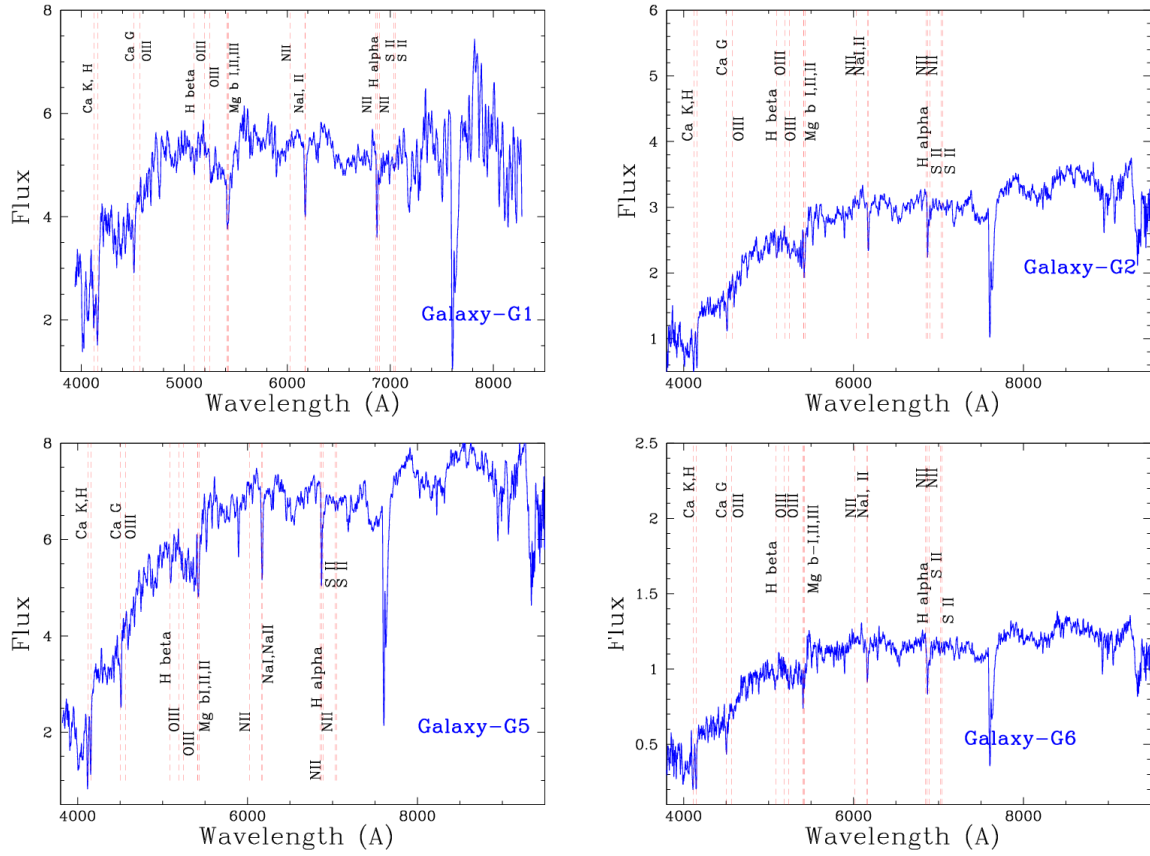


Figure 11. The optical spectra of galaxies G1, G2, G5 and G6. The spectra of members G2, G5 and G6 (the galaxies which are near the radio intensity peaks of Figure 3) were taken Palomar 200-inch Hale Telescope. The spectra of the brightest member G1 is taken using the 2-meter telescope at IUCAA Girawali Observatory. Flux scale in the y-axis is $\times 10^{-16}$ ergs $\text{cm}^{-2} \text{s}^{-1} \text{\AA}^{-1}$.

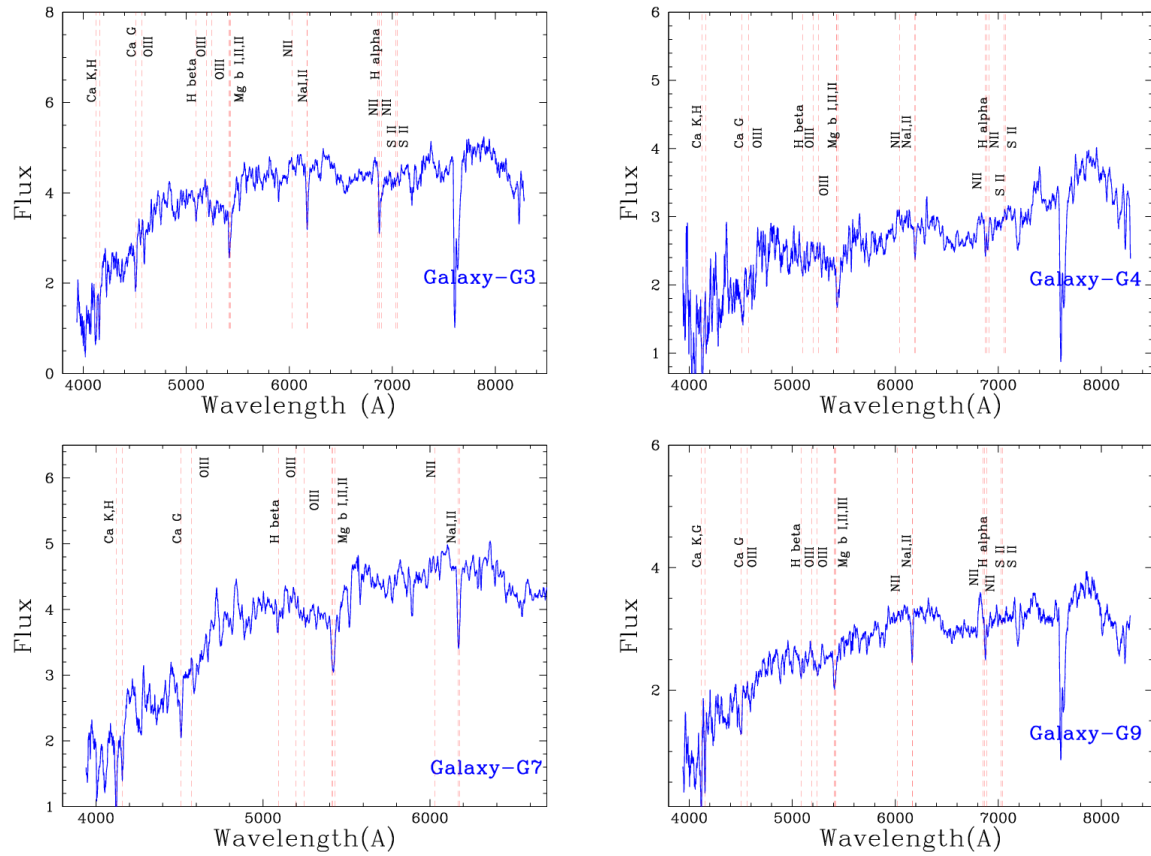


Figure 12. The optical spectra of galaxies G3, G4, G7 and G9 all taken using the 2-meter Telescope at IUCAA Girawali Observatory. Flux scale in the y-axis is $\times 10^{-16}$ ergs cm^{-2} s^{-1} \AA^{-1} .